

Cavity-enhanced absorption spectroscopy of molecular oxygen

Livio Gianfrani

*Dipartimento di Scienze Ambientali della Seconda Università di Napoli
and Istituto Nazionale per la Fisica della Materia, Unità di Napoli Via Arena, 22, I-81100, Caserta, Italy*

Richard W. Fox and Leo Hollberg

National Institute of Standards and Technology, 325 Broadway, Boulder, Colorado 80303

Received February 3, 1999; revised manuscript received May 28, 1999

A high-finesse optical cavity was employed to perform highly sensitive spectroscopy of molecular oxygen at wavelengths near 763 nm. An equivalent absorption length of ~ 1 km was obtained by a 26-cm-long optical cavity with a finesse of 6000. An extended cavity diode laser was frequency locked to the cavity, and pure absorption profiles were recovered by monitoring of the cavity transmission during continuous scans of the cavity resonance through O_2 rotational lines, allowing a detailed investigation of the line shapes. Phase modulation of the laser at a frequency equal to the cavity free-spectral-range frequency was employed for detection of weak absorption signals inside the cavity. A minimum detectable absorption coefficient of $6.9 \times 10^{-11} \text{ cm}^{-1} \text{ Hz}^{-1/2}$ was measured. Finally, a test of the symmetrization postulate in ^{16}O nuclei was demonstrated. [S0740-3224(99)00112-5]

OCIS codes: 300.1030, 300.6360, 120.2230.

1. INTRODUCTION

High-finesse cavities are a powerful tool for sensitive laser spectroscopy, since the effective absorption path length can be 100–1000 times greater than commonly used multipass cells. A number of methods have been used to monitor absorption in the cavity, including measurement of the cavity decay and the cavity transmission and the use of radio-frequency (RF) techniques. Cavity ring-down spectroscopy has been widely used to measure cavity decay times and hence absorption.^{1–3} Initially investigated with pulsed lasers, cavity ring-down spectroscopy has been extended to single-mode cw dye lasers⁴ and cw extended-cavity diode lasers.^{5,6} More recently, the application of heterodyne detection to cavity ring-down spectroscopy has dramatically increased the sensitivity to the point of approaching shot-noise-limited detection levels.⁷

The most direct approach to measure absorption in a high-finesse cavity is simply to measure a change in the transmitted power. With this method a detection limit of 10^{-8} cm^{-1} has been reported for C_2H_2 detection⁸ in a non-tunable 46-cm-long Fabry–Perot cavity, with a finesse of ~ 18000 . In that experiment the cavity transmission was monitored while the laser was tuned through the cavity modes that were coincident with the absorption line, allowing the acquisition of a few points over a Doppler-broadened profile. As we show in this paper, with the laser frequency locked to a tunable cavity, the transmitted power can be recorded during continuous frequency scans of the cavity resonance over the absorption line. However, the residual fluctuations of the laser frequency with respect to the cavity resonance are converted to amplitude noise, which makes it difficult to achieve good sensi-

tivity, and this becomes even more of a problem as the effective path lengths are increased.

A significant reduction in the spectrometer's detection limits can be obtained by RF heterodyne techniques in the detection of the transmitted power. In particular, a heterodyne cavity-enhanced technique has been recently demonstrated to detect weak saturated absorption signals inside an optical cavity.^{9,10} This method, which has been called NICE-OHMS, or noise-immune cavity-enhanced optical heterodyne molecular spectroscopy,¹⁰ is based on frequency modulation of the laser beam at the cavity free-spectral-range (FSR) frequency or a multiple of the FSR. An absorption detection limit of 10^{-14} cm^{-1} in the detection of narrow saturated absorption features has been reported,¹⁰ with a cavity finesse of 10^5 . This result is one of the most sensitive absorption measurements ever reported, to our knowledge, by any technique to date.

As with optical heterodyne spectroscopy without the optical cavity, the signal arises when a sideband is differentially absorbed or when dispersion causes a phase shift of the carrier or sidebands. Residual fluctuations of the laser power and frequency will affect the transmitted carrier but will also lead to exactly the same variations in the intensity and phase of the transmitted sidebands. The signal derived from the synchronous detection of the transmitted power at the FSR is relatively immune to laser frequency fluctuations, as compared with the direct approach.

Doppler-broadened absorption profiles of C_2HD overtone transitions near $1.064 \mu\text{m}$ have been measured in this manner by temperature tuning a Nd:YAG laser and locking onto successive cavity transmission peaks around an absorption line.¹¹ The molecular linear dispersion

was recorded by counting the frequency of the RF source that was locked to the cavity FSR. This scheme was also proposed in Ref. 12, and numerical simulations on CH₄ at 1.651 μm , CO₂ at 1.563 μm , CO at 1.567 μm , and NO₂ at 0.8 μm demonstrated how gas concentrations at the part-per-trillion level could in principle be measured with an optical cavity with a finesse of 10 000.

An extension of this heterodyne cavity-enhanced technique to measure the full Doppler or pressure-broadened shape may find applications in the field of molecular spectroscopy, in trace-gas detection, and in the detection of forbidden transitions. However, there are complications associated with extension of the extreme detection limit of 10^{-14} cm^{-1} to wider wavelength scans required for Doppler- and pressure-broadened lines. The widths of such lines (~ 1 GHz) are of the same magnitude as spurious interference fringes common in laser spectroscopy (100 MHz to 10 GHz). It can be expected that any such fringes will negatively affect the detection limit compared with that of a narrow saturated feature. In addition, even modest wavelength scans require an optical cavity capable of scanning microns of length. Measuring wider spectra may require repeated relocking of the laser to different cavity fundamental modes and acquisition of the spectra in a piecewise fashion.

Here we report an implementation of the heterodyne cavity-enhanced (CE) technique in which we continuously measure spectra up to 8 GHz (0.27 cm^{-1}) wide. Although this is broad enough for our measurement purposes in O₂, the present scan range is limited by the piezoelectric actuators of the cavity, and wider scans should be possible

with different actuators. To monitor absorption in the cavity, we synchronously detect the transmitted power at the FSR frequency. Continuous cavity scans are made through absorption lines, with the laser source always locked to the cavity resonance. We employed a 26.4-cm-long half-symmetric cavity in a stainless-steel chamber that could be pumped down and filled with O₂. Weak magnetic-dipole transitions of the $b^1\Sigma_g^+(v' = 0) \leftarrow X^3\Sigma_g^-(v'' = 0)$ band,¹³ around 762 nm, were measured. We performed a test of accuracy and sensitivity by recording heterodyne signals at very low oxygen pressures. Recordings of ¹⁶O¹⁸O and ¹⁶O¹⁷O magnetic-dipole lines in natural abundant samples provided a further demonstration of the low detection limits of our spectrometer. We also report a detailed experimental investigation of pure absorption profiles provided by the direct observation of the cavity transmitted light. The theory of a Fabry-Perot cavity in the presence of an absorbing medium is also reviewed. Finally, we discuss the possibility of using our spectrometer to improve the upper limit to a possible violation of the symmetrization postulate in the oxygen spectrum, of several orders of magnitude with respect to the values recently set.^{14,15}

2. EXPERIMENTAL SETUP

The experimental apparatus is shown in Fig. 1. We use a single-mode antireflection (AR) coated diode laser that emits at a wavelength of 776 nm at room temperature, mounted in a grazing-incidence extended-cavity configuration that was 13 cm long.¹⁶ By lowering the diode tem-

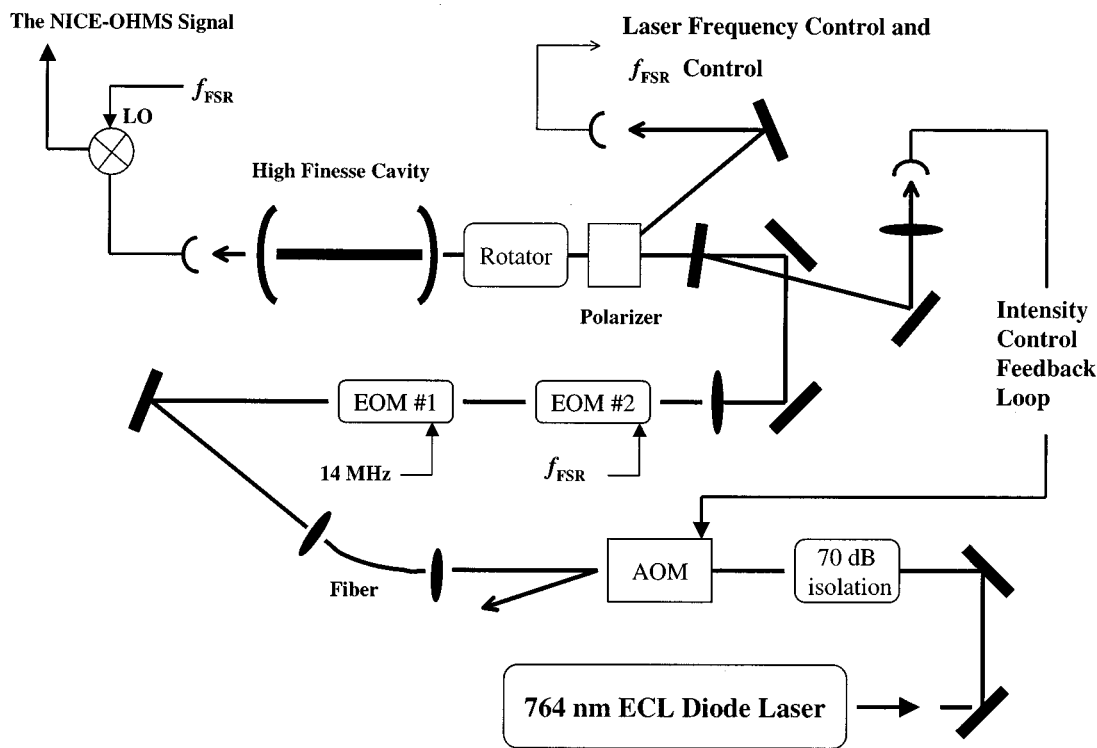


Fig. 1. Heterodyne CE experimental setup. The cavity reflection is used to lock the laser to the m th cavity mode and to lock the RF source to the cavity free spectral range. The acousto-optic modulator (AOM) is used to reduce low-frequency-intensity noise. The sidebands from electro-optic modulator (EOM) #2 are transmitted through the $(m - 1)$ and $(m + 1)$ fundamental cavity modes and detected with a high-speed photodetector, in a manner analogous to RF heterodyne spectroscopy.

perature and adjusting the grating, we could tune the laser wavelength down to 762 nm, hence covering most of the oxygen band. The spectral characteristics of extended-cavity lasers are well known. Typically they have an inherent fast linewidth of ~ 10 kHz, but they also have a large amount of frequency noise or jitter at acoustic frequencies. Relatively slow (~ 1 -MHz bandwidth) electronic feedback can tightly lock such a laser to the center of a high-finesse cavity, as described below.

The optical path from the laser to the cavity included two phase modulators, two optical isolators, and an optical fiber. The 50-cm-long single-mode optical fiber was used in the beam path as a spatial filter in order to facilitate the mode matching of the laser light into the cavity. The use of the fiber decoupled any adjustments of the laser from the alignment into the cavity and more importantly, the alignment through the phase modulators. The fiber ends were angle polished to avoid reflections, and the fiber was followed by a polarizer to fix the output polarization angle.

The optical resonator had a FSR of 568 MHz and was constructed with a 100-cm-radius input coupler and a flat output mirror. Scanning was accomplished by means of three piezoelectric transducer stacks mounted between the input mirror and the invar cavity spacer. Each stack was capable of $8\ \mu\text{m}$ of motion with 150 V applied, and the stacks were arranged on a diameter 120° apart, operated in compression, and driven in parallel. No change in the resonance peak height that would indicate a misalignment was observed as up to 14 longitudinal cavity modes were scanned past the laser frequency. An empty-cavity finesse of 6000 was found from a measurement of the cavity-mode linewidth. The cavity was mounted in a stainless-steel vacuum chamber with Brewster-angled windows, into which high-purity oxygen gas could be filled at adjustable pressures and pumped out with an oil-free vacuum pump system. We monitored the pressure with an uncertainty of <10 mTorr using a capacitance manometer (and also using a Pirani gauge as a check).

The laser source was frequency locked to the cavity with the Pound–Drever–Hall method,¹⁷ with sidebands at ~ 14 MHz with an amplitude of $\sim 5\%$ of the carrier. Phase-sensitive detection of the cavity-reflected beam provided a dispersion signal that was used to feed back to the laser injection current and the external cavity length, by means of a fast and a slow servo amplifier, respectively. We measured a bandwidth of the fast loop of ~ 1.5 MHz. With the laser locked to the cavity, sweep and dither signals used to modulate the cavity were also sent to the laser in a feedforward manner.

In the presence of an absorbing gas, direct absorption profiles could be recorded with the dc output of the fast photodetector monitoring power transmitted through the cavity. This served as a means to calibrate accurately the effective path length of the cavity by scanning across lines with a known absorption coefficient.

The RF sidebands at 568 MHz were impressed by electro-optical modulator 2, a resonant single-loop *LC* tank circuit driven by 300 mW of RF power.¹⁸ The capacitance was dominated by the crystal, an AR-coated $5\ \text{mm} \times 5\ \text{mm} \times 50\ \text{mm}$ long piece of LiNbO_3 . Because the FSR changes by a small amount as the cavity is

scanned (by approximately $2\ \text{kHz}/\mu\text{m}$ of mirror motion), this necessitated locking of the 568-MHz RF source to the FSR. The reflected power from the cavity is higher when the sidebands are reflected, thus dithering the RF frequency about the FSR and demodulating the cavity reflection at the dither frequency results in a lock signal.¹⁰ The 568-MHz frequency was dithered at 70 kHz, and the feedback loop bandwidth was ~ 10 kHz. Both the dither rate and the loop bandwidth were limited by the RF sweep generator employed. We note that a dither rate as low as 70 kHz is not optimum in this case, since the diode laser exhibits a relatively large amount of noise in this frequency region. It is also possible to derive an error signal for this lock from the sum or difference frequencies of the two phase modulators.¹⁹ In our case that would entail demodulation of the cavity reflection at 554 MHz, which is the difference between the FSR and the Pound–Drever–Hall lock frequency. This is a much lower noise region of the spectrum and should result in improved performance.

The cavity transmission was monitored with a wide-band (1-GHz) detector. The high-frequency portion of the photocurrent from the cavity transmission was bandpass filtered, demodulated at 568 MHz, lowpass filtered, and sent to a data-acquisition system. The phase of the 568-MHz local oscillator was adjusted so that dispersion-like signals were observed when the cavity mode was scanned over an absorption line. This is the heterodyne CE signal. As with heterodyne detection without a cavity, the signal level will fluctuate with changes in the phase modulation imparted to the light beam. We can suppress resulting noise and baseline changes by using a modulation of the CE signal and then demodulating subsequent to the high-frequency RF demodulation. We did this by using a dither of the cavity. As the cavity was slowly swept over the spectral region of interest, a sine modulation was superimposed on the cavity piezo drive signal. The rate was typically 50 Hz, with a modulation depth corresponding to approximately 500 MHz of optical frequency. The modulation depth was limited by broadening of the observed lines, and the rate was limited by the servo gain bandwidth of the loop holding the RF modulation on the FSR frequency. Using a lock-in amplifier, we observed the first derivative of the dispersion-like profile by demodulating at 50 Hz.

High-quality optical components with good AR coatings were used. They were carefully mounted in order to avoid spurious interference effects caused by residual backreflections.

Unfortunately, when the laser frequency was locked to the cavity, the electronic corrections of the servo on the laser injection current increased the intensity noise inside the loop bandwidth.²⁰ In principle, this should not affect the noise background of the signal demodulated at the FSR from the cavity transmission. In practice, the phase modulator produces some residual amplitude modulation at the FSR, the magnitude of which is dependent on the laser intensity. We reduced this source of noise using an acousto-optic modulator in a feedback loop (~ 100 -kHz bandwidth) to control the laser power. A beam splitter and detector before the cavity sampled $\sim 1/3$ of the power, and the acousto-optic modulator was used to deflect

power from the fiber input so as to keep the sampled power constant.

3. THEORY

In the presence of an absorbing medium the optical field transmitted through a Fabry–Perot cavity is given by

$$\frac{E_t(\nu)}{E_0} = t_1 t_2 \exp(i2\pi c t/\lambda) \exp(i2\pi n l/\lambda) \times \frac{\exp(-\alpha(\nu)L/2)}{1 - r_1 r_2 \exp(i4\pi n L/\lambda) \exp(-\alpha(\nu)\rho L)}. \quad (1)$$

Here, E_0 is the field amplitude incident upon the cavity, λ is the laser wavelength, L is the optical cavity length, and n is the refractive index. $\alpha(\nu)$ is the pressure-dependent absorption coefficient of the absorbing medium in $\text{cm}^{-1} \text{Pa}^{-1}$, p is the pressure, and t_1 , t_2 , and r_1 , r_2 are the amplitude-transmission and reflection coefficients for the input and output mirrors.

When the laser frequency is resonant with the cavity, in the limit of $\alpha(\nu)\rho L \ll 1$ and $r_{1,2} \approx 1$, the fraction of the power transmitted over the incident power may be written as

$$\frac{P_t(\nu)}{P_0} = \frac{t_1^2 t_2^2}{(1 - r_1 r_2)^2} \frac{1}{\left[1 + \frac{\alpha(\nu)\rho L \sqrt{r_1 r_2}}{1 - r_1 r_2}\right]^2}. \quad (2)$$

The equation above, after a simple algebraic calculation, provides the fractional change in the transmitted power caused by the lossy medium:

$$\frac{\delta P_t(\nu)}{P_t} = 1 - \frac{1}{\left[1 + \frac{\alpha(\nu)\rho L \sqrt{r_1 r_2}}{1 - r_1 r_2}\right]^2}. \quad (3)$$

If the one-pass absorption loss $\alpha(\nu)\rho L$ is much lower than the empty cavity loss $1 - r_1 r_2$, Eq. (3) becomes

$$\frac{\delta P_t}{P_t}(\nu) = 2\alpha(\nu)\rho L \frac{\sqrt{r_1 r_2}}{1 - r_1 r_2}. \quad (4)$$

Comparing Eq. (4) with the Beer–Lambert law, we may conclude that the absorption path length is enhanced by a factor $2F/\pi$, where F is the empty-cavity finesse, given by

$$\frac{\pi \sqrt{r_1 r_2}}{1 - r_1 r_2}.$$

Thus an equivalent interaction length L_{eq} can be defined as

$$L_{\text{eq}} = \frac{2}{\pi} FL. \quad (5)$$

It is worth noting that the Doppler-broadened absorption profile is a Gaussian function only in the limit of validity of Eq. (4). Otherwise, Eq. (2) must be used to predict the line shape observed.

4. RESULTS

A. Pure Absorption Spectroscopy

Pure absorption profiles, corresponding to the $^P P(9)$ line at 763.8434 nm, were recorded for several values of the oxygen pressure, always keeping the laser source frequency locked to the cavity. The results are shown in Fig. 2. In spite of the large frequency scans (greater than 5 GHz), a flat background was observed in each spectrum. This is the case even though the laser power was changing appreciably over the scan owing to the characteristics of the extended-cavity laser. Indeed, the intensity control feedback loop was able to cancel any change in the laser power during the cavity scans. We also note that the laser remained locked to the cavity even in the case in which the transmittance was less than 10%. The total fractional change in the transmittance at the line center was measured as a function of the O_2 pressure, and is shown in Fig. 3. The saturation of the signal at higher pressure demonstrates that spectrometers that employ cw-cavity-enhanced spectroscopy are capable of a large dynamic range and still enjoy a linear response at low levels of absorption.

Using Eq. (3), we found a nearly perfect fit of the experimental data, as shown in the same figure. Since the absorption coefficient of this line at line center and room temperature, $\alpha(\nu_0)$, is well known,²¹ we were able to deduce from the fit an accurate measurement of L_{eq} : 962 (± 2) m. This value is necessary to determine an accurate calibration of the spectrometer sensitivity. Also, knowledge of L_{eq} enables the measurement of unknown absorption coefficients. For instance, we repeated the same experimental procedure, as shown in Figs. 2 and 3, for the $^P Q(13)$ line at 764.6304 nm. Using the above reported value of L_{eq} , we found an absorption coefficient $\alpha(\nu_0)$, at room temperature, of $4.54(6) \times 10^{-8} \text{ cm}^{-1} \text{ Pa}^{-1}$ ($6.06 \times 10^{-6} \text{ cm}^{-1} \text{ Torr}^{-1}$), which is in agreement with the value reported in Ref. 22.

The absorption line shape of the transmitted power versus wavelength is provided by Eq. (2). This is demon-

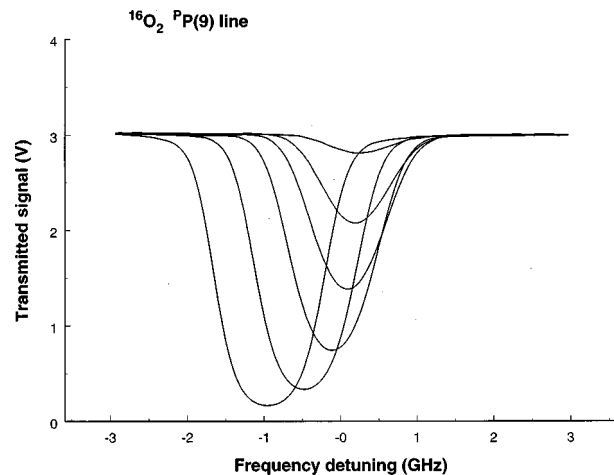


Fig. 2. Directly detected transmitted power from the cavity as the system is scanned over an oxygen absorption line. The six traces are with pressures of 13.3, 106.7, 173.3, 400, 800, and 1333 Pa. The shift in the absorption is primarily the cavity shifting that is due to the increasing refractive index with O_2 pressure. The departure from a Doppler line shape is due to the decrease in the effective path length with increasing cavity loss.

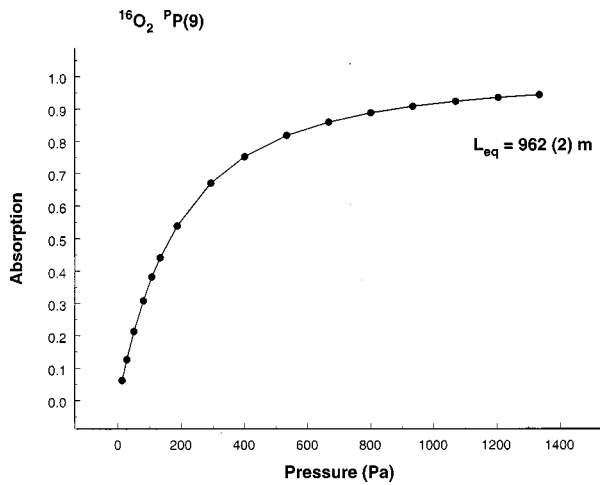


Fig. 3. Peak absorption of the $^{16}\text{O}_2$ $P(9)$ line as a function of pressure. The system response is linear if the absorption that is due to the gas is much less than the mirror loss and saturates with increasing absorption as the effective path length is reduced. A fit of these data with the theory (see text) results in an accurate determination of the effective path length, nearly 1 km in this case.

strated in Fig. 4, where a good fit of the spectrum corresponding to an O_2 pressure of 533 Pa (4 Torr) is shown. An attempt to fit the experimental points with a Gaussian function shows a clear disagreement. Indeed, in this case the Beer–Lambert law [Eq. (4)] cannot be used because the single-pass absorption $\alpha(\nu_0)pL$, equal to 7.3×10^{-4} , is comparable to $1 - r_1r_2$, which is $\sim 5 \times 10^{-4}$. However, a slight asymmetry in the line shape occurs, as evidenced in the residuals shown in the upper part of Fig. 4. This may well be due to nonlinearities of the scan owing to the piezoelectrics moving the mirror. A more accurate determination of line shapes would require some sort of linearization of the cavity scan. We note that, in principle, this information is available if the FSR frequency is monitored because a linear scan in optical frequency results in a linear scan of the FSR. However, the deviations of the data from Eq. (2) could also be due in some part to thermally induced changes in the refractive index of the absorbing gas. If the refractive index is changed by Δn , the cavity resonance is shifted by

$$\Delta \nu_m = -\nu_m \Delta n. \quad (6)$$

Therefore even if we attempt to change linearly the cavity resonance frequency ν_m about an absorption line by using a linear voltage ramp and well-behaved piezoelectric actuators, further changes in ν_m are introduced by the absorbing medium, giving rise to a slight nonlinear scan. Similar effects are often observed owing to nonzero values of $\Delta n/\Delta T$ in frequency-doubling crystals in build-up cavities. Also, this effect has been investigated in the near-IR spectrum of oxygen and acetylene.²³ In that case a free-running laser source was employed and asymmetric cavity resonances were observed when the laser frequency was resonant with the sample gas. However, these effects were much smaller in oxygen, likely because of the slow collisional energy relaxation.

A more evident effect, owing to refractive-index changes, can be noted in Fig. 2, in which the frequency

shift of the cavity resonance with respect to the absorption line increases with the oxygen pressure inside the chamber. The refractive index increases with the pressure, leading to a displacement of the cavity resonance toward the red. The pressure shift of the line center makes a contribution much smaller than the observed shift (the pressure-shift coefficient²⁴ is ~ 3.8 kHz/Pa (0.5 MHz/Torr)). Although thermal drift of the cavity length could contribute to the observed shift, we experimentally verified that it is negligible on the time scale of our measurement. From a fit of each spectrum the line center was determined as a function of the oxygen pressure. A linear fit of the experimental points shown in Fig. 5 provides a displacement rate of 0.910(3) MHz/Pa. We performed these measurements also for the $P(13)$ line and found a shift of 0.899(9) MHz/Pa. The uncertainties correspond to one standard deviation. These shifts correspond to a change in the index of refraction of approximately 2.3 nPa^{-1} ($3 \times 10^{-7} \text{ Torr}^{-1}$).

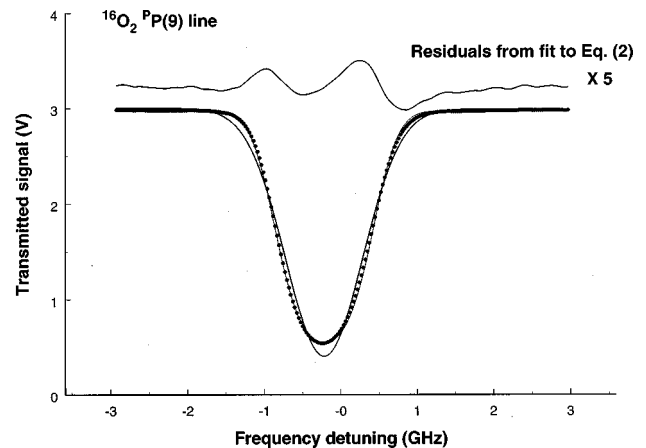


Fig. 4. Dots are data points taken from one trace of Fig. 2. The oxygen pressure is 533 Pa. A least-squares fit of the theory [Eq. (2)] to the data is shown as a thin solid curve nearly on top of the data points. The residuals from the fit are shown above with a $5\times$ magnified scale. A least-squares fit of a Doppler line shape to the data is also shown.

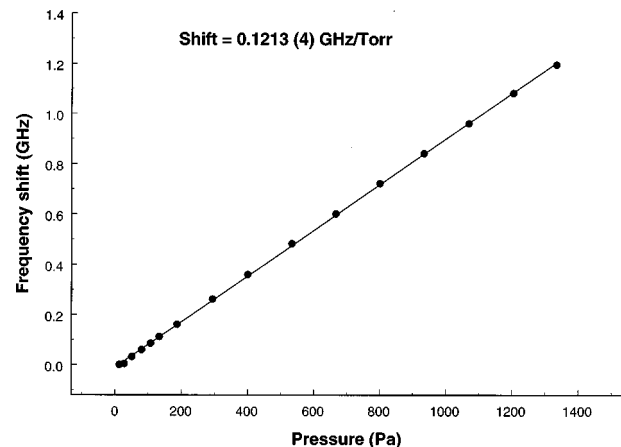


Fig. 5. Data points are the frequency shift of the apparent absorption line shape as a function of the oxygen pressure and are shown along with a best-fit straight line. The data points were determined from best fits of the Fig. 2 data series to Eq. (2). The shift is primarily due to the increasing index of refraction.

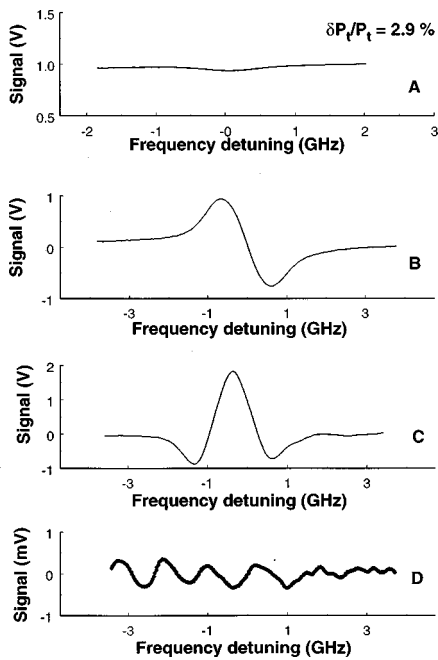


Fig. 6. Trace A is the direct photocurrent detected from the cavity transmission while scanning over the $^PQ(13)$ line of $^{16}\text{O}_2$ with 50 mTorr of pressure. Trace B is the heterodyne CE signal, the demodulation of the photocurrent at the free-spectral-range frequency. Trace C is the demodulation of the CE signal with a lock-in while the cavity was slowly modulated and swept over the absorption. Trace D is the noise baseline in a nearby spectral region that has no known absorptions. Traces B, C, and D are 10 coadditions (see text).

B. Heterodyne Measurements

The heterodyne CE measurement should be far superior to a direct absorption measurement, since the laser has less noise at higher frequencies and less residual frequency noise is converted to amplitude noise by the cavity. Four signal traces are shown in Fig. 6 that illustrate the heterodyne versus the direct measurement. The first three were recorded with 6.67 Pa (50 mTorr) of oxygen in the cavity, while trace D was recorded with four times that pressure.

Trace A shows the direct absorption corresponding to the $^PQ(13)$ line of $^{16}\text{O}_2$. The absorption coefficient at line center is $3.0 \times 10^{-7} \text{ cm}^{-1}$, measured by recording of an absorption of 2.9% over the 962-m path.

Trace B is the heterodyne CE signal from the cavity-transmitted power. The cavity output was detected with a wideband detector, and the resulting photocurrent was synchronously detected at the modulation frequency, which was locked to the cavity's FSR.

Trace C also represents the heterodyne CE signal but is recorded by a slow (50-Hz) modulation of the cavity frequency as the resonance is swept over the absorption line. After synchronous detection at the FSR frequency, a lock-in amplifier is used to demodulate the 50-Hz signal. This second demodulation serves to reject fluctuations of the modulation index, for instance, caused by noise of the RF power source. The resulting line shape is the derivative of Trace B.

Finally, trace D is a magnified portion of the baseline, away from any known signals. It is evident the system is limited by systematic noise.

We note that simply evacuating the cavity to determine the baseline would not be sufficient, because oxygen absorption in the ambient air path to the cavity is readily observed. An analysis of the detection sensitivity can be done accurately only if the laser source is tuned to a wavelength region where no absorption features occur. Trace D was taken at a wavelength free from any overlapping magnetic-dipole lines of oxygen isotopomers, i.e., $^{16}\text{O}^{18}\text{O}$, $^{16}\text{O}^{17}\text{O}$, $^{17}\text{O}^{18}\text{O}$, $^{18}\text{O}_2$, and $^{17}\text{O}_2$, as can be verified with the data reported in Refs. 25 and 26.

The noise is clearly due to spurious interference fringes, mainly caused by the residual reflectivity of the AR-coated facets of EOM#2. An accurate signal-to-noise (S/N) measurement requires the estimation of the noise level in the background signal. If the background noise were random, we could measure the ratio between the amplitude of the signal and the root-mean-square of the background. However, the background is still dominated by systematic fringes, and we measure a S/N ratio of 8000 by graphically comparing trace C, divided by the S/N, and trace D. More explicitly, the peak in trace C may still be recognized as a signal when trace C is divided by 8000 and added to trace D. Since trace C represents an absorption at line center of $3 \times 10^{-7} \text{ cm}^{-1}$, the measured absorption detection limit was $\alpha_{\text{min}} = 3.8 \times 10^{-11} \text{ cm}^{-1}$.

Traces B, C, and D were recovered with a cavity-transmitted power of 500 μW , a low-pass filter bandwidth B of 3 Hz, and 10 coadditions. Coadditions refers to averaging of N spectral traces together to reduce the random-noise component by \sqrt{N} . Each individual data trace exhibited more noise fluctuations than is evident in trace D. In fact, it was only by averaging that we could observe the fringes clearly. Therefore we find the equivalent absorption detection limit on a per hertz basis with no coadditions by multiplying the measured limit by \sqrt{N} and dividing by \sqrt{B} . This measured absorption detection limit is $6.9 \times 10^{-11} \text{ cm}^{-1} \text{ Hz}^{-1/2}$.

Under shot-noise-limited operation, the theoretical minimum detectable single-pass absorption is given by¹⁰

$$\left. \frac{\delta P_t}{P_t} \right)_{\text{single pass}}^{\text{min}} = \alpha_{\text{min}} L = \frac{\pi}{2F} \sqrt{\frac{2eB}{\eta P_t J_0(\beta) J_1(\beta)}} \frac{1}{\sqrt{2}}, \quad (7)$$

where the modulation index β was approximately 0.5, the empty-cavity finesse $F = 6000$, the cavity-transmitted power $P_t = 500 \mu\text{W}$, and the photodiode responsivity $\eta = 0.5 \text{ A/W}$. Normalizing Eq. (7) with respect to the bandwidth yields a theoretical shot-noise-limited detection level of $5.8 \times 10^{-11} \text{ Hz}^{-1/2}$, equivalent to a minimum detectable absorption coefficient of $2.2 \times 10^{-12} \text{ cm}^{-1} \text{ Hz}^{-1/2}$. Thus our present detection limit is approximately a factor of 30 above the shot-noise limit.

C. O_2 Forbidden Transitions

Trace D of Fig. 6 was recorded by scanning of the cavity resonance around the calculated position of the oxygen $^{16}\text{O}_2$ $^PP(12)$ forbidden line at 764.5088 nm. In the O_2 spectrum, transitions starting from even rotational quantum numbers are missing. This is a consequence of the symmetrization postulate of quantum mechanics. This phenomenon has been used to perform a test of the sym-

metrization postulate,^{14,15} and an upper limit to a possible violation in O₂ has previously been set at 5×10^{-7} .

The spectral region around the ¹⁶O₂ ^PP(12) line was explored in the presence of 2.67×10^4 Pa (200 Torr) of oxygen inside the chamber. No evidence of a signal in the expected position of the ^PP(12) line was found. Thus after a comparison with trace C of Fig. 6, considering the S/N ratio, scaling the observed signals for the different values of the pressure, and also taking into account the pressure broadening of the lines, we found an upper limit to the intensity of the ^PP(12) forbidden line with respect to the ^PQ(13) line of 5×10^{-8} . This is factors of 10 and 16 smaller than the respective limits reported in Refs. 14 and 15.

We also observed weak lines of ¹⁶O¹⁸O and ¹⁶O¹⁷O isotopomers in natural abundance oxygen samples (atomic abundance: ¹⁸O = 0.2%, ¹⁷O = 0.037%). In Fig. 7 the heterodyne CE signal corresponding to the ^PQ(13) line at 764.4890 nm of ¹⁶O¹⁷O isotopomer is recorded for four values of the oxygen pressure, from 667 Pa to 1.33×10^4 Pa. In Fig. 8 the peak amplitude of these signals is plot-

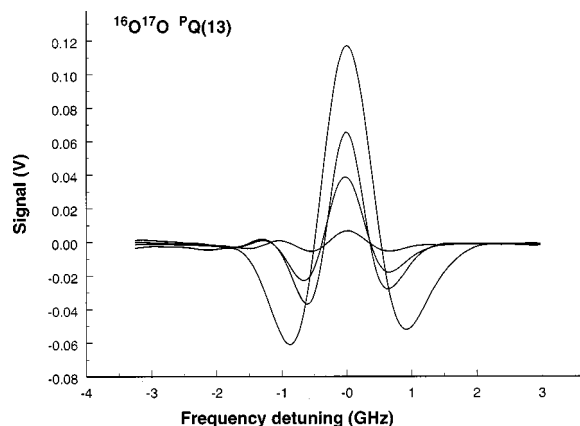


Fig. 7. NICE-OHMS signal from absorption of the ^PQ(13) line of ¹⁶O¹⁷O at 764.489 nm for four different pressures of natural-abundance oxygen (from 660 Pa up to 1.3×10^4 Pa).

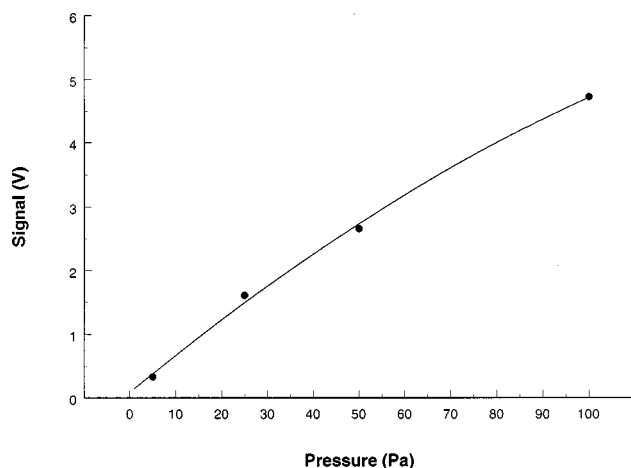


Fig. 8. Peak signal levels from Fig. 7 plotted as a function of pressure. A best-fit simple polynomial curve is shown also. The slight nonlinearity is due to pressure broadening and the decreasing modulation width, not to saturation of the NICE-OHMS signal.

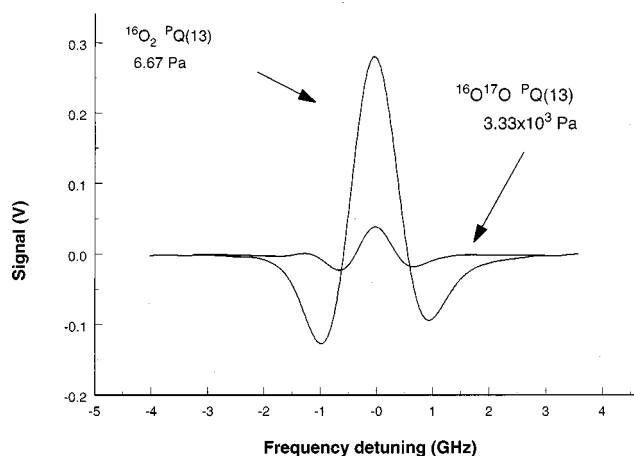


Fig. 9. Comparison of the signal from a ¹⁶O₂ line with a known absorption coefficient allows the determination of the absorption coefficient of the ¹⁶O¹⁷O line. This is given by the ratio between the amplitude of the two signals (~ 0.16) times the absorption coefficient of the ¹⁶O₂ line ($4.54 \times 10^{-8} \text{ cm}^{-1} \text{ Pa}^{-1}$) and is divided by the partial pressure of the ¹⁶O¹⁷O measurement relative to the ¹⁶O¹⁶O measurement (0.38). The natural molecular fractional abundance of ¹⁶O¹⁷O is 7.6×10^{-4} .

ted as a function of the pressure, and a slight nonlinear behavior can be noted. This is due to two factors: the onset of pressure broadening and the decreasing modulation width from the constant dither amplitude. In Fig. 9 a comparison between the ^PQ(13) lines in ¹⁶O¹⁷O and ¹⁶O₂ enables the measurement of the absorption coefficient $\alpha(\nu_0)$, at room temperature, for the ¹⁶O¹⁷O line. It was found to be $1.91(3) \times 10^{-8} \text{ cm}^{-1} \text{ Pa}^{-1}$.

5. CONCLUSIONS

We have extended the cavity-enhanced (or NICE-OHMS) technique to the Doppler-limited regime by recording signals continuously over frequency spans up to 8 GHz. Using an equivalent path length of 962 m, we observed weak magnetic-dipole transitions of molecular oxygen around 762 nm. Absorption profiles were continuously recovered with the laser locked to the cavity by scanning of the cavity resonance frequency through the line. We also presented an investigation of the line shapes from the interaction of the intracavity laser radiation with Doppler-broadened lines.

Our sensitivity corresponds to a minimum detectable absorption coefficient of $6.9 \times 10^{-11} \text{ cm}^{-1} \text{ Hz}^{-1/2}$. Although this is the lowest detection limit obtained in the laboratory for the molecular oxygen near-IR absorption spectrum, if we consider the recent experiments in Refs. 14, 15, 25, and 26, it is still a factor of 30 from the shot-noise level that should be achievable. The dominant noise in this experiment was due to residual interference fringes from optical components. An improvement may be provided by incorporation of a Brewster-cut crystal in the FSR phase modulator instead of the AR-coated one used here. Another possible source of the systematic background is deviations of the 568-MHz sidebands from the cavity FSR. Realizing the RF lock servo in a different manner may result in a higher S/N ratio and better performance.

Further improvements to the sensitivity are possible by an increase in the mirror reflectivity. Available low-loss mirrors easily support a cavity finesse of 6×10^4 , which would provide an order-of-magnitude improvement of the sensitivity. Although the resulting cavity linewidth (~ 10 kHz) would be comparable with the inherent laser linewidth, there is enough electronic gain available to collapse nearly all the power into the cavity lock.

Our spectrometer enabled an improvement of the upper limit to a possible violation of the symmetrization postulate in the $^{16}\text{O}_2$ spectrum. In this paper, we have set a value of 5×10^{-8} , which is a factor 10 better than in previous work with O_2 .

ACKNOWLEDGMENTS

The authors are grateful to J. Ye, L.-S. Ma, and J. L. Hall for their helpful assistance, including the designs of the resonant modulator and high-speed detectors used in this work. This work is a contribution of the U.S. Government, and is not subject to copyright.

REFERENCES AND NOTES

1. A. O'Keefe and D. A. G. Deacon, "Cavity ring-down optical spectrometer for absorption measurements using pulsed laser sources," *Rev. Sci. Instrum.* **59**, 2544–2551 (1988).
2. D. Romanini and K. K. Lehmann, "Ring-down cavity absorption spectroscopy of the very weak HCN overtone bands with six, seven, and eight stretching quanta," *J. Chem. Phys.* **99**, 6287–6301 (1993).
3. J. B. Paul, J. J. Scherer, A. O'Keefe, and R. J. Saykally, "Cavity ringdown measures trace concentrations," *Laser Focus World* **33**, 71–75 (1997).
4. D. Romanini, A. A. Kachanov, N. Sadeghi, and F. Stoeckel, "CW cavity ring down spectroscopy," *Chem. Phys. Lett.* **264**, 316–322 (1997).
5. D. Romanini, A. A. Kachanov, and F. Stoeckel, "Diode laser cavity ring down spectroscopy," *Chem. Phys. Lett.* **270**, 538–545 (1997).
6. B. A. Paldus, C. C. Harb, T. G. Spence, B. Wilke, J. Xie, J. S. Harris, and R. N. Zare, "Cavity-locked ring-down spectroscopy," *J. Appl. Phys.* **83**, 3991–3997 (1998).
7. M. D. Levenson, B. A. Paldus, T. G. Spence, C. C. Harb, J. S. Harris, and R. N. Zare, "Optical heterodyne detection in cavity ring-down spectroscopy," *Chem. Phys. Lett.* **290**, 335–340 (1998).
8. K. Nakagawa, T. Katsuda, A. S. Shelkovnikov, M. de Labacherie, and M. Ohtsu, "Highly sensitive detection of molecular absorption using a high finesse optical cavity," *Opt. Commun.* **107**, 369–372 (1994).
9. J. Ye, L.-S. Ma, and J. L. Hall, "Sub-Doppler optical frequency reference at $1.064 \mu\text{m}$ by means of ultrasensitive cavity-enhanced frequency modulation spectroscopy of a C₂H₂ overtone transition," *Opt. Lett.* **21**, 1000–1002 (1996).
10. J. Ye, L.-S. Ma, and J. L. Hall, "Ultrasensitive detections in atomic and molecular physics: demonstration in molecular overtone spectroscopy," *J. Opt. Soc. Am. B* **15**, 6–15 (1998).
11. J. Ye, "Ultrasensitive high resolution laser spectroscopy and its application to optical frequency standards," Ph.D. dissertation (University of Colorado, Boulder, Colorado, 1997).
12. A. Mugino, T. Tamamoto, T. Omatsu, M. A. Gubin, A. Morinaga, and N. Takeuchi, "High sensitive detection of trace gases using optical heterodyne method with a high finesse intra-cavity resonator," *Opt. Rev.* **3**, 243–250 (1996).
13. H. D. Babcock and L. Herzberg, "Fine structure of the red system of atmospheric oxygen bands," *J. Astrophys.* **108**, 167–190 (1948).
14. M. de Angelis, G. Gagliardi, L. Gianfrani, and G. M. Tino, "Test of the symmetrization postulate for spin-0 particles," *Phys. Rev. Lett.* **76**, 2840–2843 (1996).
15. R. C. Hilborn and C. L. Yuca, "Spectroscopic test of the symmetrization postulate for spin-0 nuclei," *Phys. Rev. Lett.* **76**, 2844–2847 (1996).
16. The laser was an SDL 5400C (mentioned to specify experimental parameters; other sources may be suitable).
17. R. W. P. Drever, J. L. Hall, F. V. Kowalski, J. Hough, G. M. Ford, A. J. Munley, and H. Ward, "Laser phase and frequency stabilization using an optical resonator," *Appl. Phys. B* **31**, 97–105 (1983).
18. L.-S. Ma, JILA, University of Colorado, Boulder, Colorado (personal communication, 1997).
19. R. G. DeVoe, C. Fabre, K. Jungmann, J. Hoffnagle, and R. G. Brewer, "Precision optical-frequency-difference measurements," *Phys. Rev. A* **37**, 1802–1805 (1988).
20. R. W. Fox, L. D'Evelyn, H. G. Robinson, C. S. Weimer, and L. Hollberg, "Amplitude modulation on frequency-locked extended-cavity diode lasers," *Proc. SPIE* **2378**, 58–62 (1995).
21. M. de Angelis, L. Gianfrani, F. Pavone, A. Sasso, and G. M. Tino, "Temperature dependence of self-broadening in molecular-oxygen spectrum," *Nuovo Cimento* **18**, 557–564 (1996).
22. K. J. Ritter and T. D. Wilkerson, "High-resolution spectroscopy of the oxygen A-band," *J. Mol. Spectrosc.* **121**, 1–19 (1987).
23. P. Dubé, L.-S. Ma, J. Ye, P. Jungner, and J. L. Hall, "Thermally induced self-locking of an optical cavity by overtone absorption in acetylene gas," *J. Opt. Soc. Am. B* **13**, 2041–2054 (1996).
24. A. J. Phillips and P. A. Hamilton, "Pressure-shift of the (0, 0) and (1, 0) bands of the oxygen $b^1\Sigma_g^+ - X^3\Sigma_g^-$ transition from Fourier transform spectroscopy," *J. Mol. Spectrosc.* **174**, 587–594 (1995).
25. H. Naus, A. de Lange, and W. Ubachs, " $b^1\Sigma_g^+ - X^3\Sigma_g^-$ (0, 0) band of oxygen isotopomers in relation to tests of the symmetrization postulate in O-16(2)," *Phys. Rev. A* **56**, 4755–4763 (1997).
26. G. Gagliardi, L. Gianfrani, and G. M. Tino, "Investigation of the $b^1\Sigma_g^+(\nu = 0) < -X^3\Sigma_g^-(\nu = 0)$ magnetic-dipole transitions in O-18(2)," *Phys. Rev. A* **55**, 4597–4600 (1997).